Electronic Supplementary Material (ESI) for Journal of Materials Chemistry A.
This journal is © The Royal Society of Chemistry 2022

# Electronic supplementary information (ESI):

## Materials

The $SnO_2$ colloid precursor was obtained from Alfa Aesar (tin (IV) oxide, 15% in $H_2O$ colloidal dispersion). Fluorine-doped tin oxide (FTO) glass substrates (sheet resistance 12 Ω /sq) were purchased from Asahi Glass Co. Ltd. The Semicon detergent, acetone, isopropanol, N, N-Dimethylformamide (DMF, 99.8%), dimethyl sulfoxide (DMSO, 99.9%), 4-tert-butyl pyridine (tBP), and chlorobenzene (CB, 99.8%) were purchased from Sigma-Aldrich. Spiro-OMeTAD (2, 2', 7, 7'-tetrakis (N, N-di-p-methoxy- phenyalmine) -9, 9' -spirobifuorene) and Cesium iodide (CsI, 99.9%) were obtained from You Xuan Tech, China. Bismuth (III) chloride ($BiCl_3$, 98%) and Bismuth (III) iodide ($BiI_3$, 98%) were purchased from Aladdin. 1,3-Bis[3,5-bis(trifluoromethyl) phenyl] thiourea was obtained from Bi De company. Lithium bis (triuoromethanesulfonyl) imide (Li-TFSI) and Acetonitrile (ACN, 99.8%) were purchased from Xi 'an Paulette and Bei 'jing Lark wei, respectively. All chemical reagents were used as received without further purification.

## Device fabrication

FTO substrates with a size of 2×2 $cm^2$ were obtained by cutting from the original a size of 36×45 $cm^2$, and then the designed pattern on FTO glass is etched by laser etching machine. The etched FTO was rinsed in an aqueous detergent solution and Semicon cleaning solution for 5 and 10 minutes, respectively, followed by ultrasonic treatment with deionized water (15 minutes), acetone (5 minutes) and isopropyl alcohol (5 minutes). The above clean FTO was dried by clean air, and treated for 15 minutes under ultraviolet/ozone (UVO) condition. $SnO_2$ colloidal solution was prepared by diluting the $SnO_2$ colloidal solution (15 wt%) to 2.14 wt% with deionized water. The above diluted $SnO_2$ solution was coated onto the FTO films by spin coating with 2500 rpm for 30 s, followed by thermal annealing at 200℃ for 40 minutes. After the films were cooled down to room temperature, the $SnO_2$ films were exposed to UVO for 10 minutes. The $CsBi_3I_{10}$ precursor solution (0.33 M) was prepared by dissolving CsI of

173.8 mg, $BiI_3$ of 1179.8 mg, and $BiCl_3$ of 44.4 mg, in the mixed solvents of 1.8 mL DMF and 0.2 mL DMSO ($V_{DMF}$: $V_{DMSO}$=9 : 1). The perovskite films were made by spin-coating the above as-prepared perovskite precursor solution on the $SnO_2$ films at 1000 rpm for 12 s, 5000 rpm for 50 s, during which 0.2 mL chlorobenzene (CB) as anti-solvent was dripped on the perovskite films at 40 s before ending the program. The wet orange perovskite films were annealed at 150 ℃ for 30 min in glovebox. For the preparation of FS modified CBI, different quantity of FS was introduced into CBI precursor according to the percentage (for example, 20% FS-modified CBI is named as 20-FS-CBI). Furthermore, the $N_2$ purge process for 20-FS-CBI was applied by blowing the $N_2$ gas directly on the film immediately after the CB anti-solvent was dropped. Spiro-OMeTAD solution was obtained by dissolving 72.3 mg spiro-OMeTAD in 1 mL chlorobenzene, and adding 28.8 mL of 4 -tert-butyl pyridine (tBP) and 17.5 mL of lithium bis(triuoromethanesulfonyl)imide (Li-TFSI) stock solution (520 mg Li-TSFI in 1 mL acetonitrile) into the above solution. The spiro-OMeTAD films were prepared through spin-coating the above as-obtained solution on the perovskite films at 3000 rpm for 30 s. Finally, a 80 nm-thick silver counter electrode was thermally evaporated on the top of the spiro-OMeTAD film under a vacuum of 6$\times 10^4$ Pa by using a shadow mask. Photovoltaic performance measurements were carried out in ambient air with a relative humidity of 30-40%) for devices without encapsulation.

**Characterization**

Current-voltage (J-V) curves were measured using a solar simulator equipped with 150 W Xenon lamp (150 W, Solar IV-150A) and a Keithley 2400 source meter. The light intensity was calibrated to AM 1.5 G one sun (100 mW $cm^{-2}$) with a NIM calibrated standard Si solar cell (QE-B1). The effective active area of the device was defined to be 0.09 $cm^2$ by using a black metal mask. The J-V curves were measured from -0.1 V to 0.8 V (forward scan) or from 0.8 V to -0.1 V (reverse scan) with a scan rate of 100 mV $s^{-1}$. Impedance spectroscopy was measured by an Electrochemical Workstation (CHI600E, China), and the data were analyzed by the Z-View program. UV-Vis absorption spectra were measured on a UV-Vis spectrometer (Shimadzu UV-2550, China). The contact angle goniometer (DSA20 model; Kreu GMBH in Germany,

Germany) was employed to measure the contact angles. The SEM images were acquired using field-emission scanning electron microscopy (JSM-7800F, Japan). The FTIR spectra were recorded with a Nicolet IS50 Infrared Fourier transform microscope by Thermo Fisher Scientific. Standard steady-state emission spectra were performed on a Fluoromax-4 instrument (Horiba Jobin Yvon) equipped with double-grating excitation and emission monochromators and a 45 W Xe lamp as a light source. Time-resolved photoluminescence (TRPL) was measured using Edinburgh FLS1000 (UK), where the excitation wavelength of TRPL was provided by a 405 nm laser. Atomic force microscopy (AFM) measurements were carried out on Asylum Research MFP-3D-BIO (US) in tapping mode. X-ray diffraction (XRD) spectra were recorded by X-ray diffraction (XRD, Bruker D8 Advance) at room temperature using Cu Kαradiation at 45 kV and 40 mA. The sample was scanned from 5 to 65° in 2θ mode at a step of 0.02°. Probe station for semiconductor device measurements were obtained on a Lake Shore CRX-6.5K.

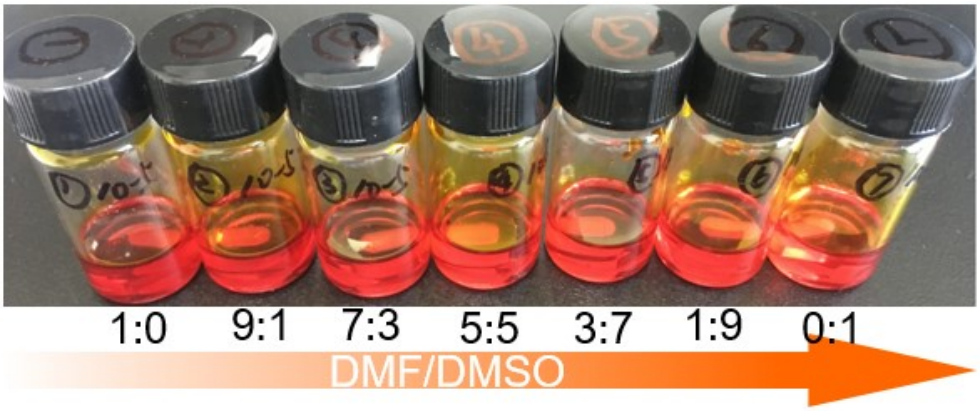


Fig. S1 Optical photographs of CBI precursor solutions with different DMF/DMSO volume ratios.

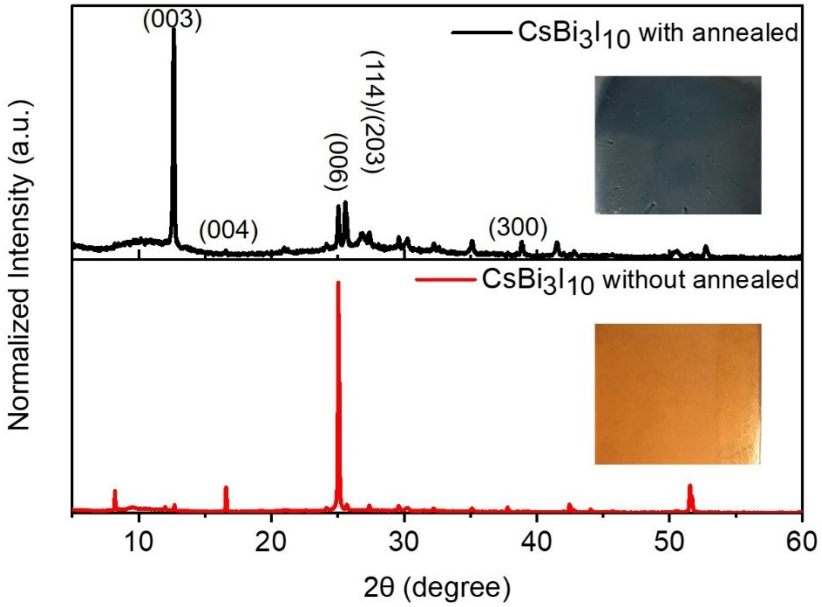


Fig. S2 X-ray diffraction (XRD) patterns of CBI with annealed and CBI without annealed (volume ratios of DMF/DMSO=9:1). Inset: photographs of pristine CBI with annealed and CBI without annealed.

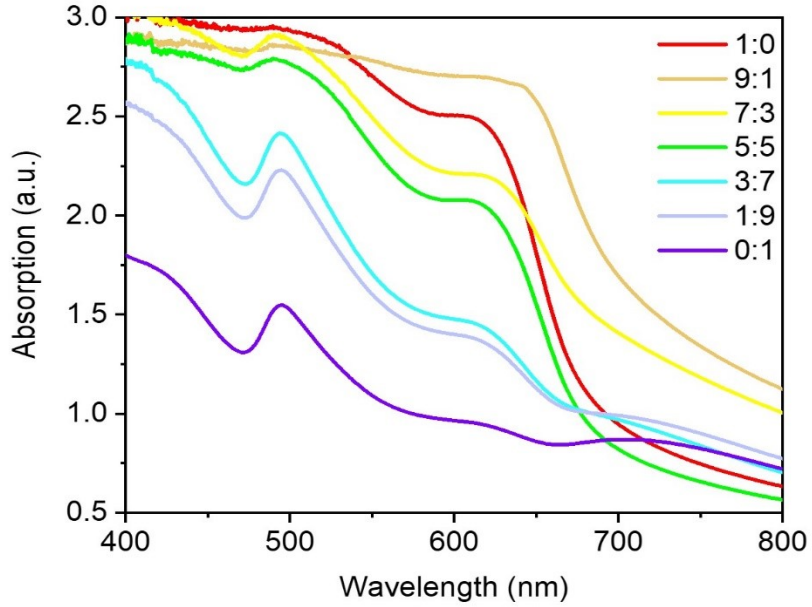


Fig. S3 Uv-vis absorption spectra of CBI films made with different volume ratios of DMF/DMSO.

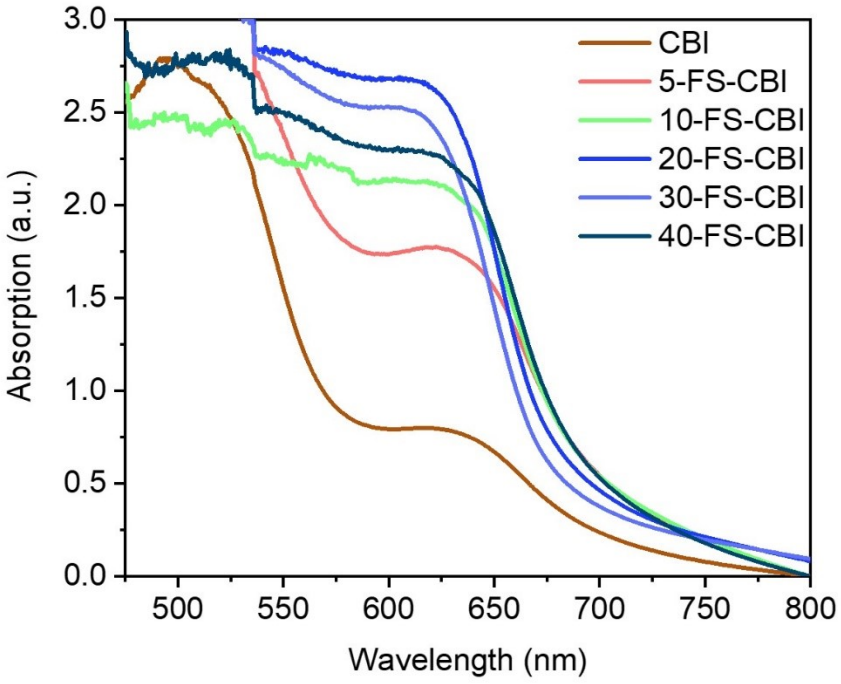


Fig. S4 Uv-vis spectra of CBI film and FS modified CBI films by different concentrations of FS.

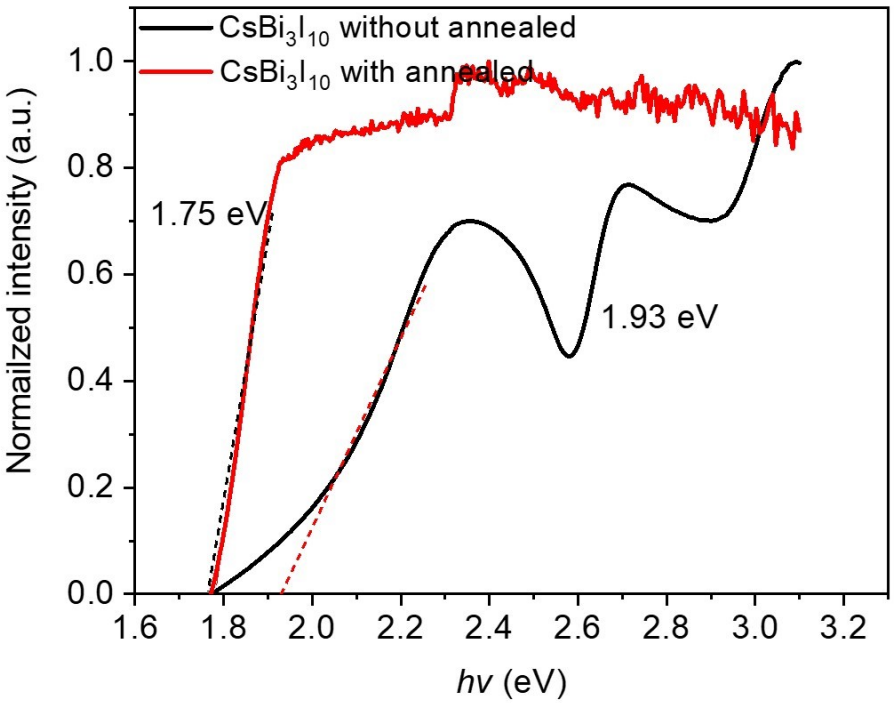


Fig. S5 Tauc plots of pure CBI with annealed and CBI without annealed.

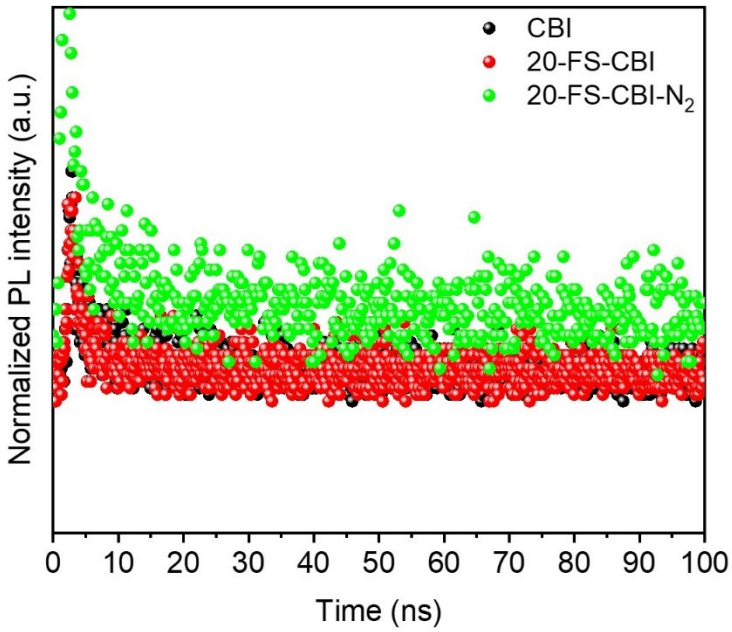


Fig. S6 Time-resolved PL decay with double-exponential fitting for CBI, 20-FS-CBI and 20-FS-CBI-$N_2$ three thin films (excitation at 405 nm).

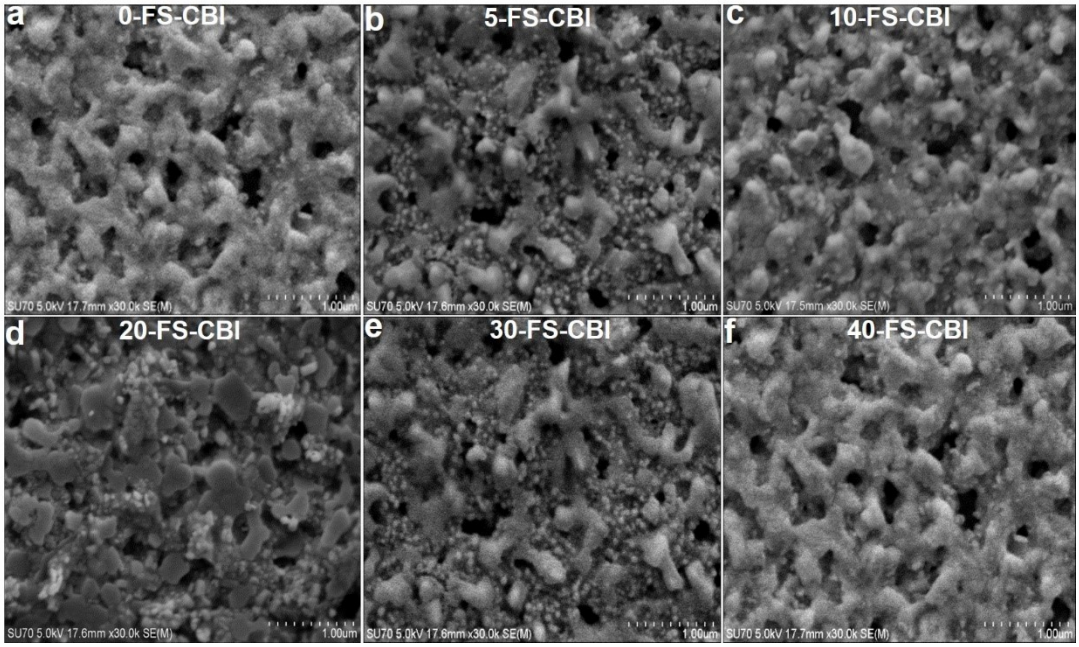


Fig. S7 (a) Scanning electron microscope (SEM) photos of (a) CBI, (b) 5-FS-CBI, (c) 10-FS-CBI, (d) 20-FS-CBI, (e) 30-FS-CBI and (c) 40-FS-CBI. The scale bar is 1 μm, respectively.

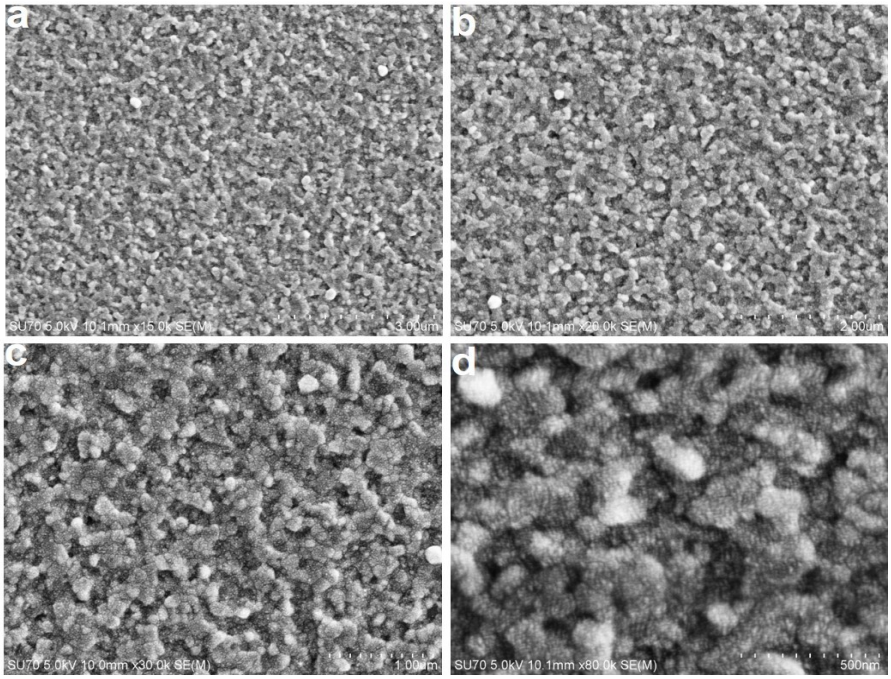


Fig. S8 SEM photos of 20-FS-CBI-$N_2$ thin films with different scale bar: (a) 3 μm, (b) 2 μm, (c) 1 μm and (d) 500 nm, respectively.

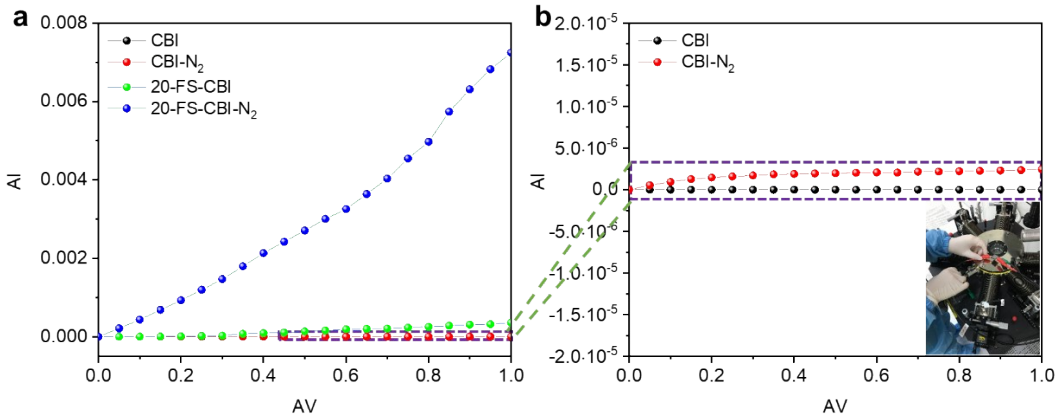


Fig. S9 (a) The resistivity of CBI, CBI-$N_2$, 20-FS-CBI and 20-FS-CBI-$N_2$. (b) The zoom-in view of resistivity of CBI, CBI-$N_2$. The inset image shows a four-probe test diagram.

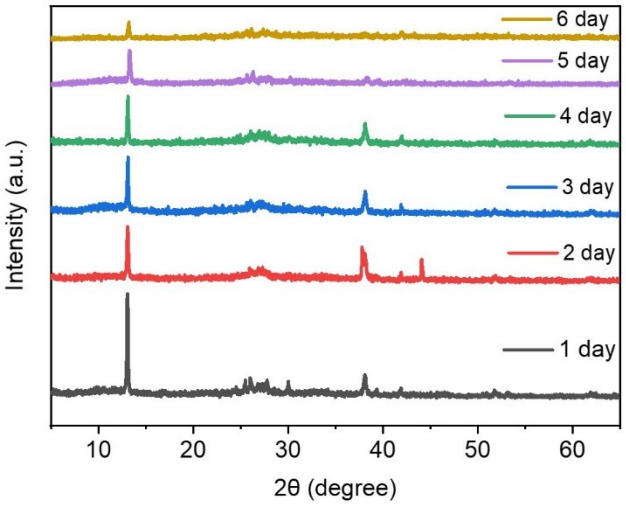


Fig. S10 XRD changes over time based on CBI thin films in ambient environment.

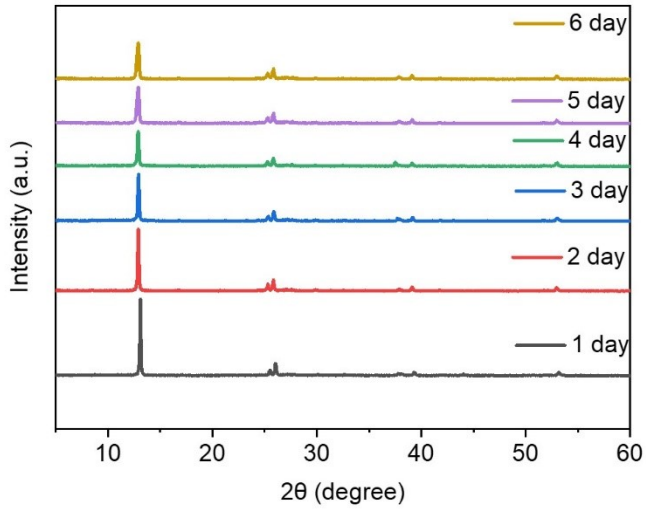


Fig. S11 XRD changes over time based on 20-FS-CBI thin films in ambient environment.

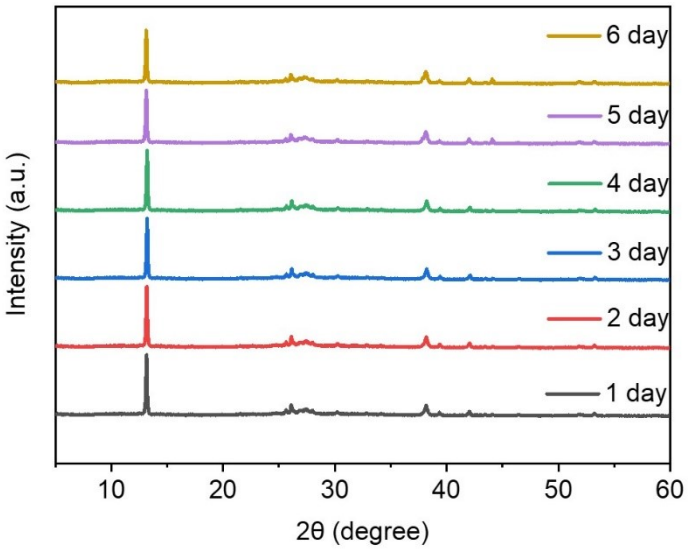


Fig. S12 XRD changes over time based on 20-FS-CBI-$N_2$ thin films in ambient environment.

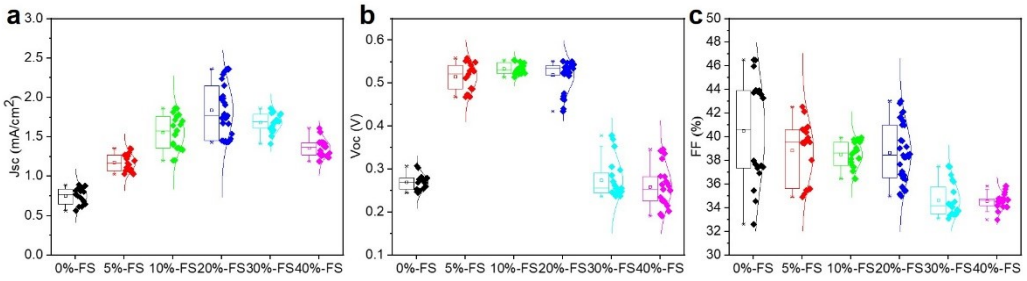


Fig. S13 Statistics of the photovoltaic parameters of CBI thin-film solar cells with different FS: (a) $J_{sc}$, (b) $V_{oc}$ and (c) FF, respectively.

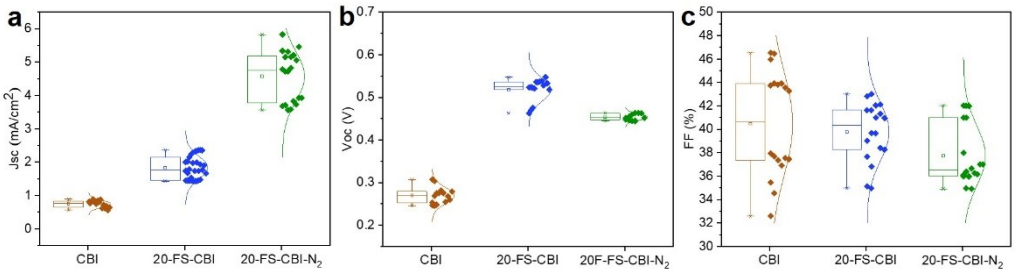


Fig. S14 Statistics of the photovoltaic parameters of bare CBI, 20-FS-CBI and 20-FS-CBI-$N_2$ thin-film solar cells: (a) $J_{sc}$, (b) $V_{oc}$ and (c) FF, respectively.

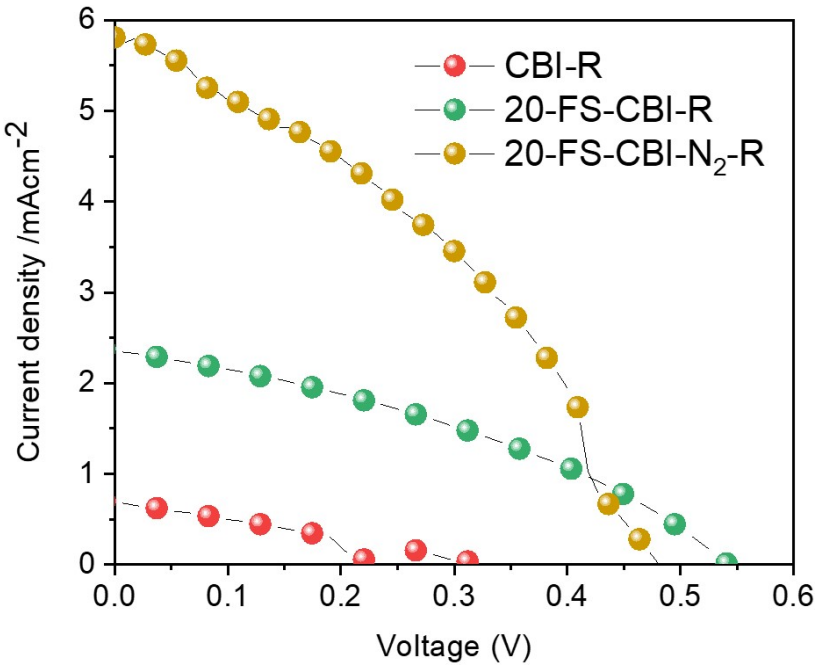


Fig. S15 Representative J-V curves of the solar cells with reverse scan based on CBI, 20-FS-CBI and 20-FS-CBI-$N_2$, respectively.

Table S1. Fitted PL lifetime of CBI, 20-FS-CBI and 20-FS-CBI-$N_2$ three thin films (excitation at 405 nm) (by bi-exponential decay).

| Samples | $\tau_{1\ (ns)}$ | $\tau_{2\ (ns)}$ | $B_1$ | $B_2$ | $\tau_{ave\ (ns)}$ |
|---|---|---|---|---|---|
| CBI | 0.1891 | 4.8474 | 57.13 | 42.87 | 2.43 |
| 20-FS-CBI | 0.9065 | 10.372 | 25.80 | 74.20 | 3.55 |
| 20-FS-CBI-$N_2$ | 0.8552 | 14.791 | 33.34 | 66.66 | 11.95 |

Notes[1]: $I(t) = I_0 + B_1\exp(-t/\tau_1) + B_2\exp(-t/\tau_2)$, where $\tau_1$ and $\tau_2$ represent fast and slow decay time constant, respectively. Average time constant ($\tau_{ave}$) is calculated using relation $\tau_{ave} = (B_1\tau_1^2 + B_2\tau_2^2)/(B_1\tau_1 + B_2\tau_2)$.

Table S2. Photovoltaic parameters statistics of the devices based on CBI, 20-FS-CBI and 20-FS-CBI-$N_2$ devices.

| Device structure | $V_{oc}$ (mV) | FF (%) | $J_{sc}$ (mA/cm$^2$) | PCE (%) |
|---|---|---|---|---|
| CBI | 269.3±52.7 | 40.48±0.02 | 0.749±0.38 | 0.086±0.016 |
| 20-FS-CBI | 518.2±21.8 | 36.78±0.39 | 1.83±0.52 | 0.365±0.097 |
| 20-FS-CBI-$N_2$ | 453.7±0.3 | 36.67±1.07 | 4.57±1.27 | 0.778±0.252 |

Table S3. Photovoltaic performance summary of the devices based on $CsBi_3I_{10}$.

| Device structure | Method | Scan direction | $V_{oc}$ (mV) | FF (%) | $J_{sc}$ (mA/cm$^2$) | PCE (%) |
|---|---|---|---|---|---|---|
| FTO/$TiO_2$/$CsBi_3I_{10}$/Spiro-OMeTAD/Ag | Solvent annealing | Forward | 0.55 | 42.0 | 4.45 | 1.03[2] |
| | | Reverse | 0.53 | 46.0 | 4.31 | 1.05 |
| ITO/$SnO_2$/$C_{60}$/$CsBi_3I_{10}$/TaTm/$MoO_3$/Au | Thermal-evaporation | -- | -- | -- | -- | 0.13[3] |
| ITO/PEDOT:PSS/$CsBi_3I_{10}$/PCBM/BCP/Au | Spin-coating | Forward | 650 | 27 | 2.20 | 0.38[4] |
| | | Reverse | 700 | 34 | 2.66 | 0.63 |
| FTO/PEDOT:PSS/$NiO_x$/$CsBi_3I_{10}$/PCBM/BCP/Au | Spin coating | Forward | 730 | 34 | 2.89 | 0.72[5] |
| | | Reverse | 670 | 33.4 | 2.69 | 0.60 |
| FTO/$TiO_2$/$CsBi_3I_{10}$/Carbon | Spin-coating | Forward | 460 | 66.07 | 4.87 | 1.47[6] |
| | | Reverse | 460 | 69.18 | 4.75 | 1.51 |
| FTO/$SnO_2$/FS-$CsBi_3I_{10}$/Spiro-OMeTAD/Ag (this work) | Gas quenching assisted antisolvent method (GQAS) | Forward | 454 | 36.67 | 5.84 | 0.971 |
| | | Reverse | 478 | 37.27 | 5.84 | 1.03 |

**References**


1 Xiong, Z.; Chen, X.; Zhang, B.; Odunmbaku, G. O.; Ou, Z.; Guo, B.; Yang, K.; Kan, Z.; Lu, S.; Chen, S.; Ouedraogo, N. A. N.; Cho, Y.; Yang, C.; Chen, J.; Sun, K., *Adv. Mater*., 2022, 2106118.

2 Liang, G.-X.; Chen, X.-Y.; Chen, Z.-H.; Lan, H.-B.; Zheng, Z.-H.; Fan, P.; Tian, X.-Q.; Duan, J.-Y.; Wei, Y.-D.; Su, Z.-H., *J. Phys. Chem. C*, 2019, **123**, 27423-27428.

3 Sebastia-Luna, P.; Gélvez-Rueda, M. C.; Dreessen, C.; Sessolo, M.; Grozema, F. C.; Palazon, F.; Bolink, H. J., *J. Mater. Chem. A*, 2020, **8**, 15670-15674.

4 Mariyappan, P.; Chowdhury, T. H.; Subashchandran, S.; Bedja, I.; Ghaithan, H. M.; Islam, A., *Sustainable Energy Fuels*, 2020, **4**, 5042-5049.

5 Mariyappan, P.; Chowdhury, T. H.; Subashchandran, S.; Bedja, I.; Ghaithan, H. M.; Islam, A., *Adv. Mater. Interfaces*, 2021, **8**, 2002083.

6 Shin, J.; Kim, M.; Jung, S.; Kim, C. S.; Park, J.; Song, A.; Chung, K.-B.; Jin, S.-H.; Lee, J. H.; Song, M., *Nano Res*., 2018, **11**, 6283-6293.